Journal Pre-proofs

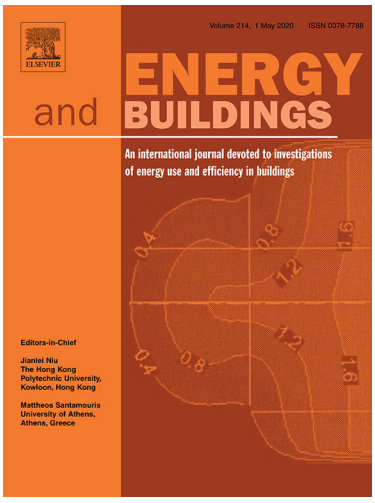

Experimental and numerical investigation of the performance of bogie chassis heater deicing systems

Mingxin Liu, Junjie Liu, Diduo Liu, Baomin Huang, Zhaojun Sun, Shen Wei, Wenhua Chen, Xingli Pu

PII: S0378-7788(19)33719-3
DOI: https://doi.org/10.1016/j.enbuild.2020.110383
Reference: ENB 110383

To appear in: *Energy & Buildings*

Received Date: 7 December 2019
Revised Date: 19 May 2020
Accepted Date: 7 August 2020

Please cite this article as: M. Liu, J. Liu, D. Liu, B. Huang, Z. Sun, S. Wei, W. Chen, X. Pu, Experimental and numerical investigation of the performance of bogie chassis heater deicing systems, *Energy & Buildings* (2020), doi: https://doi.org/10.1016/j.enbuild.2020.110383

Experimental and numerical investigation of the performance of bogie chassis heater deicing systems

Mingxin Liu [a], Junjie Liu [a, *], Diduo Liu [b], Baomin Huang [b], Zhaojun Sun [b], Shen Wei [c], Wenhua Chen [a], Xingli Pu [a]

[a] Tianjin Key Lab of Indoor Air Environmental Quality Control, School of Environmental Science and Engineering, Tianjin University, Tianjin 300072, China.

[b] China Railway Design Corporation, Tianjin 300308, China.

[c] Bartlett School of Construction & Project Management, UCL, London WC1E 7HB, UK

Corresponding author：Junjie Liu

E-mail address: jjliu@tju.edu.cn

Abstract

In winter, a large amount of icing and snowing occurs in outdoor equipment and systems, which adversely affects their lifespan. The melting process is divided into two parts: convection melting and gravity shedding melting. This paper is based on an experiment with a real high-speed train unit, and it establishes a three-dimensional computational fluid dynamics model of the bogie area to validate the mathematical model of the winter ice melting experiment. A numerical simulation was used to calculate the airflow in the baffle-enclosed space and to predict the effects of interactions between air and the ice body on heat transfer and phase change. The influence of air velocity and temperature on the heat transfer was analyzed. The computational simulation effectively quantifies the amount of heat transfer and energy consumption under different conditions. This paper also presents a research method for the simulation of gravity shedding in complex models. These models provide information for the construction of similar ice melting models. This paper has suggested that for thin ice bodies, convection melting was the dominant strategy. For thick ice

bodies, however, gravity shedding melting became dominant. The study also confirmed that enclosed hot-air ice-melting systems gave a better energy performance than unenclosed systems.

Keywords: Hot airflow, Computational Fluid Dynamics, Deicing, Energy consumption, Heat flux density

Nomenclature

S	the source term
H	enthalpy, kJ/kg
ρ	density, kg/m^3
V	velocity, m/s
h	sensible enthalpies, kJ/kg
ΔH	latent enthalpies, kJ/kg
T	temperature, °C
L	latent heat, kJ/kg
β	liquid fraction, 0~1
a	characteristic distance, m
q	heat flux density, W/m^2
t	time, s
Q	total energy, kJ
c	specific heat capacity, kJ/kg·°C
m	mass, kg
ΔT	temperature difference, °C
η	energy utilization factor

Highlights

- A new enclosed melting system was built for deicing the bottom of a train
- A new method was used for simulating gravity shedding melting in complex models
- The effect of supply air properties on system performance was studied

1. Introduction

In recent years, the number of passengers using railways in China has increased dramatically. According to [1], in 2017, the number reached 3.084 billion, with an

increase of 9.6% over 2016. In severe cold and in cold regions, however, the bogie chassis under trains may form ice when the outdoor temperature is low, as shown in Figure 1. This ice will affect the stability of system operation [2-4] and lead to serious accidents [5]. To ensure passengers' safety, it is extremely important to solve this icing issue for trains.

Figure 1: Ice on bogie chassis

Currently, four deicing methods are being used: mechanical deicing, hot-water melting, hot-air melting and ethylene glycol melting [2, 6, 7]. Except for mechanical deicing, which is achieved mainly by knocking off ice manually, all of these methods use a high-temperature medium to melt ice, and hot-air melting is most common in real applications [2, 6, 8].

Figure 2a shows a real hot-air melting system, with a schematic drawing shown in Figure 2b. In this system, two metal barriers are attached, with insulation layers to prevent release of hot air to the ambient environment. The hot air is provided by four heaters placed at the center of the rail. Using this method, heat is exchanged mainly through convection between ice and hot air, happening at the bottom of the ice. Therefore, in existing literatures[9], it has been called natural convection melting. However, when gaps exist between different pieces of ice or between the ice and the barrier, some hot air will be able to touch the train body and increase its temperature as well. The increased train-body temperature will heat the top of the ice, and some ice will drop due to gravity before fully melting by heating from the bottom. As is apparent,

this phenomenon will decrease the time required for ice melting as well as the heating energy demand. In this study, this melting mechanism has been named gravity shedding melting, and it is often neglected in real applications.

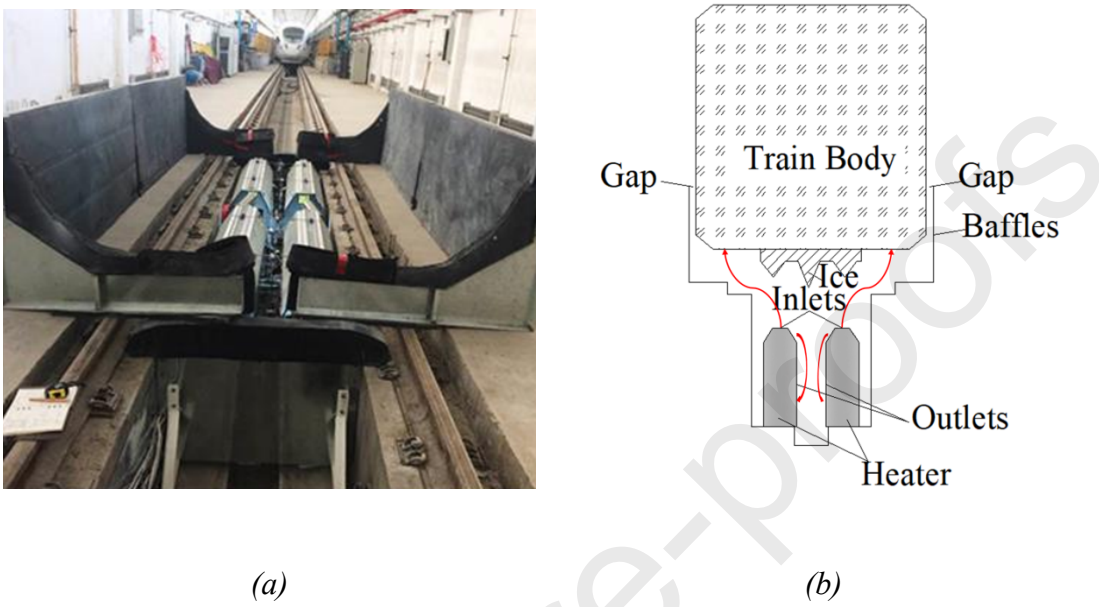

(a) *(b)*

Figure 2: A real hot-air melting system and its schematic diagram

To determine the performance of this system, simulation methods have popularly been used for predicting required heat flux and overall melting time. Compared to experimental methods, the potential advantages of simulation methods include removing the need for real materials, reducing the required labor, and increasing coordination between relevant departments [9]. According to [8, 9], mathematical models developed for solving phase-change heat conduction problems can be divided largely into two categories: multiregion models and single-region models. In multiregion models, control equations are established for each phase region, and the coincidence relationships between the solid-phase regions, the liquid-phase regions and the two-phase regions are described by establishing suitable boundary conditions at the phase interface. Multiregion models are mainly applicable to dynamic mesh technology. Single-region models are applicable to both solid-phase regions and liquid-phase regions, as well as two-phase regions. These regions are closely coupled with each other, and the simulation work can be performed using a fixed set of meshes and boundary

conditions. Due to the simplicity of single-region models, this kind of model is currently widely used in real applications.

In terms of deicing methods for trains, some relevant work has been done [2, 8, 10]. Some studies, such as [2, 8], investigated the characteristics of train deicing using simulation data. The results, however, were quite different from actual situations due to the mixture of ice and snow under trains. One study used both experimental and simulation methods carried out in a garage to investigate the best melting conditions for unenclosed hot-air ice-melting systems [10]. This study, however, released hot air into the whole garage, so a great deal of energy was used to heat the garage rather than to melt the ice. Therefore, the unenclosed systems had low the energy efficiency, and generated a lot of waste heat. Local environmental control systems have been applied in various applications, such as heating commercial buildings [11-13] and heating chairs [14], and their energy efficiency has been well proven. The enclosed hot-air ice-melting systems in this paper is a type of local environmental control systems, which generates less waste heat than unenclosed systems [15].

All existing studies [2, 8, 10] until now focused on the performance of convection melting only, and the importance of gravity shedding melting in the overall melting process has not been well justified or understood. To fill this gap in the literature, this study aimed to critically justify the importance of gravity shedding melting on the overall performance of train ice-melting systems and to develop a useful method considering this effect for future applications. This study used a new type of enclosed hot-air ice-melting system that belongs to the category of local environmental control systems, as shown in Figure 2, and both experimental work and simulation work were conducted to evaluate its performance. Additionally, a calculation method for gravity shedding melting has been proposed, based on the enthalpy-porosity technique, to benefit future system design and operation.

2. Research methods

2.1 Experimental design

2.1.1 Iron box

An iron box was used for validating both the solidification and melting model and the energy model, as well as for providing boundary conditions for modeling gravity shedding melting. In this study, the iron box was dimensioned by 200 mm×200 mm×80 mm for the thickest part of the ice was approximately 80 mm thick in the enclosed system experiment, as shown in Figure 3. Since actual high-speed train chassis often have protruding portions, this experiment used an iron bar to represent these portions. During the experiment, the ice in the iron box was frozen and placed in a heating box to remain at 40°C ± 1°C. One T-type thermocouple was placed on one side of the iron box to measure the temperature inside, with a measurement accuracy of ±0.5 K and a measurement range of -10°C to 40°C. To prevent heat loss, the iron box was wrapped with thick insulation material.

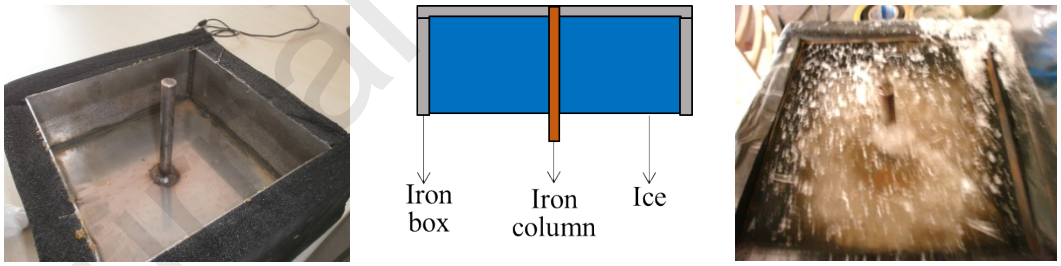

(a) *(b)* *(c)*

Figure 3: Schematic diagram and physical pictures of the iron box experiment. (a) iron box; (b) schematic diagram; (c) melting process.

2.1.2 Enclosed hot-air melting systems

The experiment on enclosed hot-air melting systems aimed to verify Computational Fluid Dynamics (CFD) models of turbulence and to provide melting time. The enclosed

hot-air melting system (shown in Figure 2) included some closed baffles and four heaters. The testing platform was mainly composed of a rail, baffles, heaters and a train unit with ice and snow. Outside the surfaces of the baffles, thick insulation material was attached to reduce heat loss to the ambient environment. In the experiment, the thickest part of the ice was approximately 80 mm. The supply air velocity was 13 m/s, with a supply air temperature of 65°C. The velocity inside the enclosed space was measured by hot-wire anemometers (TSI-8386), with a measurement range of 0~50 m/s and an accuracy of 0.01 m/s. The maximum deviation is ±3%, and the measurement range is between -10 and 60°C.

2.2 Simulation design

CFD is widely used for solving differential equations that control the fluid flow to obtain discrete distributions of the flow field over a continuous region [16]. In this study, the CFD method was adopted to model the system performance. The solutions were considered to have converged when the summation of residuals was lower than 10^{-3}, 10^{-3} and 10^{-6} for continuity, momentum and energy equations, respectively. The residuals represented relative errors in the calculation of a particular variable to measure convergence. All simulations in this study were carried out in ANSYS Fluent, a popular commercial simulation package [17-19].

2.2.1 Model development and identification of boundary conditions

Geometric model for the iron box

The dimensions of the model are detailed in Section 2.1.3, and the thickness of the ice layer was defined as 80 mm. Figure 4 depicts the geometric model.

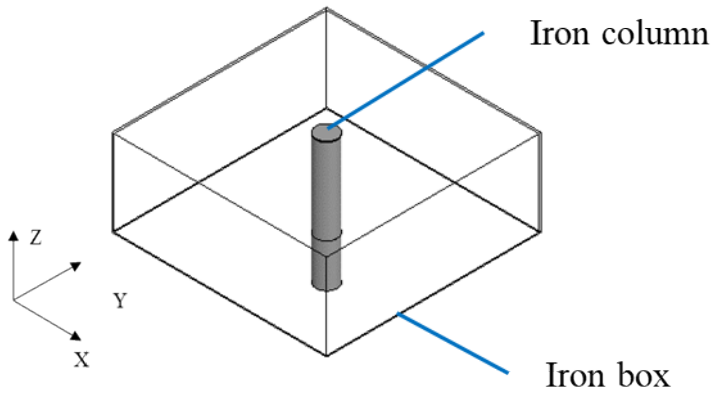

Figure 4: The iron box model

Convection-melting ice model

The convection-melting ice model retained the main geometric features of the experimental platform with the train body simplified as a wall (the bottom of the train). Both the inner air and ice layer were enclosed in a closed space, and there was a 1 mm ice layer below the bottom of the train. An overview is shown in Figure 5.

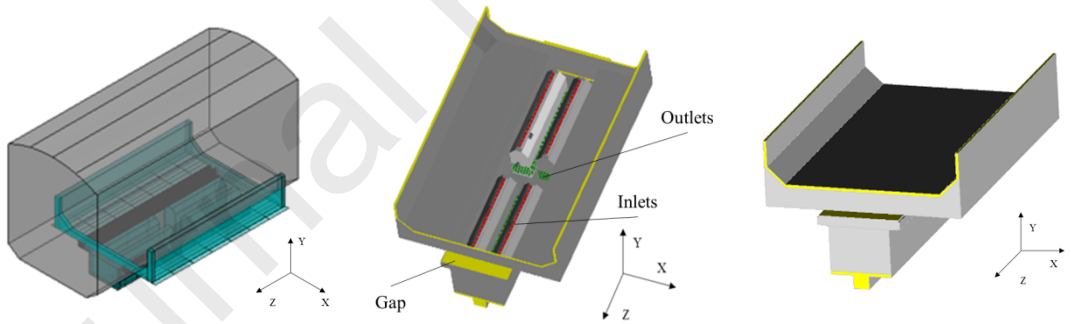

(a) *(b)* *(c)*

Figure 5: Convection-melting ice model. (a) system sketch diagram; (b) internal geometric structure (gaps: yellow; heater inlets: red; heater outlets: green); (c) external geometry structure

Gravity shedding melting model

Both the heaters and the enclosed parts of the gravity shedding melting model were

defined in the same way as the convection-melting ice model. Since there were heat-transferring parts for the train body, the model needed to be simplified. The simplified model retained the main structure, which was at the bottom of the train body, as shown in Figure 6a.

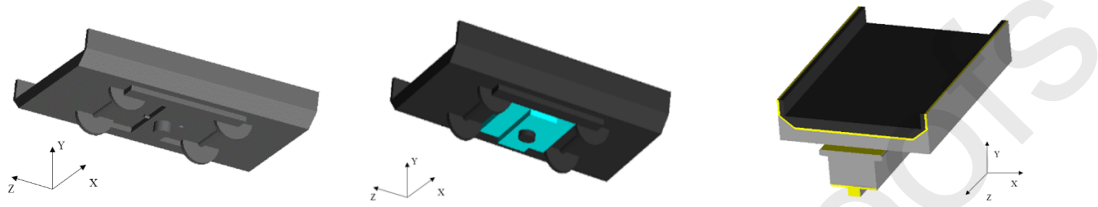

(a) *(b)* *(c)*

Figure 6: Schematic diagram of the gravity shedding melting model. (a) the simplified model of the train body; (b) ice layers (blue); (c) external geometry structure (gaps: yellow)

Boundary conditions

Table 1 shows the boundary conditions used in the CFD simulation, defined according to actual situations.

Table 1: Boundary conditions for the CFD simulation.

	Boundary parameters	Conditions
Iron box model	Exposed iron column	Surface at 40°C
	Iron box top/front/back/left/right	Surface heat flux at 0 W/m^2
	Ice	Initial temperature at -2°C
Convective melting model	Heater outlets	Pressure outlet
	Gap	Pressure outlet
	Ice	Initial temperature at -2°C
	Wall	Surface heat flux at 0 W/m^2
Gravity shedding melting model	Heater outlets	Pressure outlet
	Gap	Pressure outlet
	Ice	Initial temperature at -2°C
	Wall	Surface heat flux at 0 W/m^2

2.2.1 Calculation method

In this study, the enthalpy-porosity technique was adopted to simulate the melting process for ice. It has been widely used in various fields, such as thermal systems integrated with phase change materials [19-24]. This method uses the liquid fraction to represent the degree of melting in the solution area [19, 21, 23, 24], which is calculated by an enthalpy balance. The liquid fraction is a value between 0 and 1, with 0 for pure solid ice and 1 for pure liquid water.

Equations 1 and 2 define both mass and momentum equations,

$$\frac{\partial \rho}{\partial t} + \nabla \cdot \left(\rho \cdot \vec{V}\right) = 0 \quad (1)$$

$$\rho\left[\frac{\partial \vec{V}}{\partial t} + \left(\vec{V} \cdot \nabla\right)\vec{V}\right] = -\nabla P + \nabla \cdot \left(\mu \nabla \vec{V}\right) + S \quad (2)$$

where S is the source term.

The energy balance equation is defined by Equation 3,

$$\frac{\partial}{\partial t}(\rho H) + \nabla \cdot \left(\rho \vec{V} H\right) = \nabla \cdot (k \nabla T) + S \quad (3)$$

where $H, \rho, \vec{V}$ are material enthalpy (kJ/kg), material density (kg/m^3) and fluid velocity (m/s), respectively.

The material enthalpy is the sum of both sensible and latent heat, calculated by Equation 4,

$$H = h + \Delta H \quad (4)$$

where h and ΔH are sensible and latent enthalpies (kJ/kg).

According to the basic theory of thermodynamics, the sensible enthalpy can be written as in Equation 5,

$$h = h_{ref} + \int_{T_{ref}}^{T} C_p dT \quad (5)$$

where h_{ref} (kJ/kg) is the reference enthalpy at the reference temperature T_{ref} (°C).

The latent heat can be calculated by Equation 6,

$$\Delta H = \beta L \quad (6)$$

where L (kJ/kg) is the material's latent heat and β is the liquid fraction defined by Equation 7,

$$\beta = \begin{cases} 0 & if \quad T \le T_{solidus} \\ \frac{T - T_{solidus}}{T_{liquidus} - T_{solidus}} & if \quad T_{solidus} < T < T_{liquidus} \\ 1 & if \quad T \ge T_{liquidus} \end{cases} \tag{7}$$

2.2.3 Grid independence study

Iron box model

To determine a reasonable grid quantity for the model to save computational time, a mesh study was necessary. According to the results of the mesh study, the difference between the average side-surface temperature for cases with 0.9 and 1.5 million elements was found to be 0.08%. Since the difference was minor, a grid size of 0.9 million was retained. The grid of the iron box model is shown in Figures 7a and 7b.

Convection melting ice model

According to the results of the mesh study, the difference between the average outlet velocity in the gap for cases with 1.6 and 3.6 million elements was found to be 0.13%. In addition, the difference for the average gap outlet temperature was found to be 0.08%. Therefore, a grid size of 1.6 million was retained due to these minor differences. The grid of the convection melting model is shown in Figure 7c.

Gravity shedding melting model

Grids with 2.3, 5.9 and 8.7 million cells were selected for the grid independence study. The difference between the average of gap outlet velocity for cases with 2.3, 5.9 and 8.7 million elements were 0.23% and 0.07%, respectively, and they were 0.18% and 0.06%, respectively, for average of gap outlet temperature. Because of these minor differences, a grid size of 5.9 million was maintained. The grid of the gravity shedding melting model is depicted in Figure 7d.

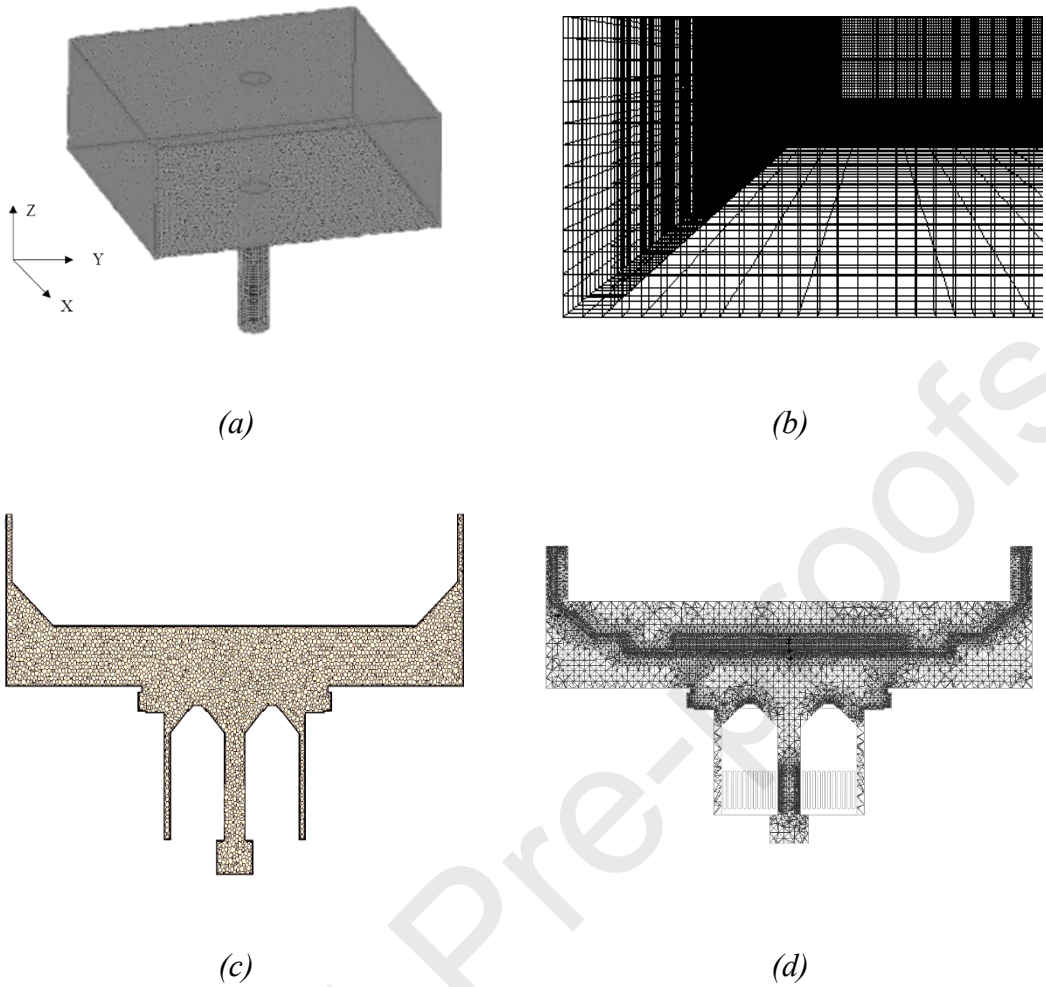

Figure 7: Distribution of the grid. (a) Iron box model; (b) a portion of the iron box model; (c) convection melting ice model; (d) gravity shedding melting model.

2.2.4 Model validation

According to the general algorithm used for calculating windshield defrosting in the automotive industry [3, 9, 25], the calculations for the deicing process were performed in two steps in this study. The first step was to calculate the steady flow field in the air region, including both velocity and temperature fields, to obtain the air region parameters for heat exchange with ice in the air region state. Based on the calculation results from step 1, the transient calculation was begun; in this calculation, the ice region was coupled with the previously calculated air region. The ice body gradually

melts according to the heat exchange capacity at different positions to obtain the resulting melting degree at each moment of the deicing process. This algorithm can predict the melting process quickly and efficiently under the condition of limited computing resources, and it was conducive to the convergence of numerical calculations and a guaranteed error range.

Turbulence model

Most studies on hot-air melting of ice have used either the RNG k-ε model or the standard k-ε turbulence model, with the RNG k-ε turbulence model being considered the most efficient and economical model for simulating indoor air flow in ground buildings [26, 27]. Many comparative studies have shown that the RNG k-ε turbulence model is superior to the standard k-ε turbulence model in overall simulation performance, and it is widely used for airflow simulation for enclosed environments [26-28]. Wu et al. [10] have used the RNG k-ε turbulence model to simulate unenclosed hot-air ice-melting systems and have obtained suitable design schemes under several working conditions.

To verify the reliability of the turbulence model for ice-melting systems, the measured values from the experiment were compared with the simulated values, with measured points shown in Figure 8. Since the measuring points should be positioned in advance, they could not be rearranged after the train body arrived. In this study, two points were positioned at the bottom of the train because of the limited number of instruments. The comparison results are shown in Figure 9. Comparing the X velocity (velocity in the horizontal direction) between experimental and simulation values, the average error was found to be 26% in the Standard k-ε turbulence model, and it was 17% in the RAN k-ε turbulence model. It can be seen that the simulated values agreed well with the experimental values, so it was believed that the RAN k-ε turbulence model had accuracy and reliability for use in this study.

In the first step, the coupling of pressure and momentum equations was achieved using

the SIMPLE algorithm. In the second step, unsteady state calculation was completed using the PISO algorithm. Because of the high Reynolds number of turbulent flow, the RAN k-ε turbulence model in the Reynolds time-average equation (RAN) of two-equation models was used. The melting phase-transformation process was modeled by the "enthalpy method" porous medium [29] model. The differential discretization had a first-order upwind difference format. The solid wall was the nonslip wall.

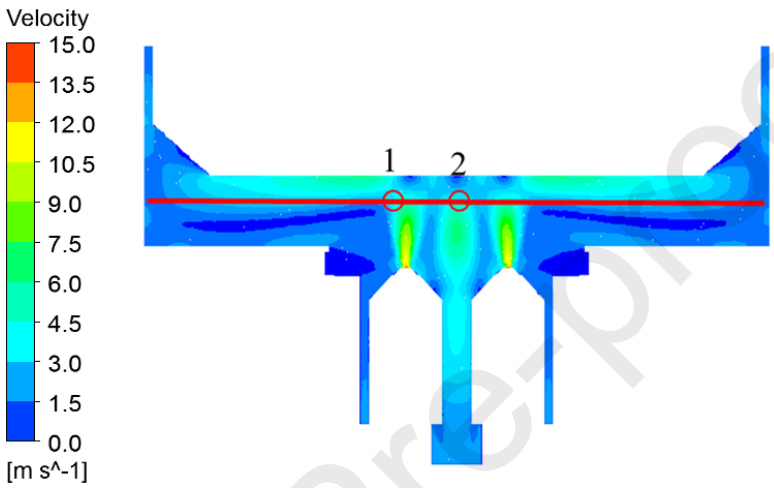

Figure 8: Velocity diagram of the experimental point cross-section

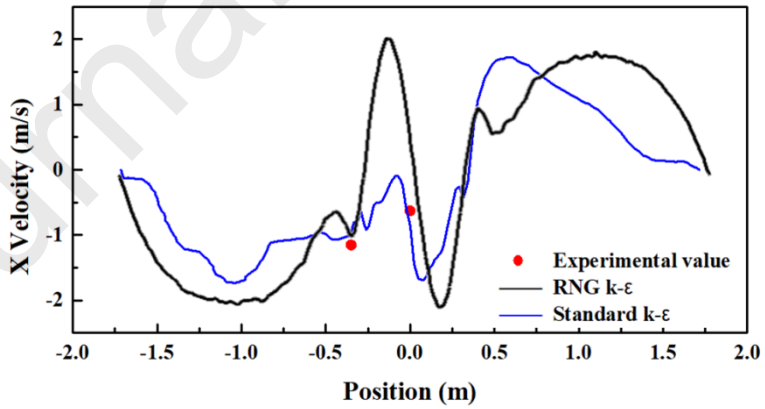

Figure 9: Changes in the vector magnitude of horizontal velocity (X velocity) with position

The solidification melting model and the energy model

The solidification melting model in FLUENT is capable of simulating a solid-liquid phase change in both pure and mixed materials; therefore, it was used for simulating the ice melting process in this study. Additionally, for the ice melting process with heat conduction, energy equations in FLUENT were used.

To verify the reliability of the solidification melting model and the energy model for ice-melting systems, both wall temperature and air temperature were compared for between their monitored values and predicted values, in Figure 10 and Figure 11, respectively. The comparisons gave an average absolute deviation of 0.7 K for wall temperature and of 1.5 K for air temperature, indicating good agreements between the two datasets and adequate prediction accuracy of the model.

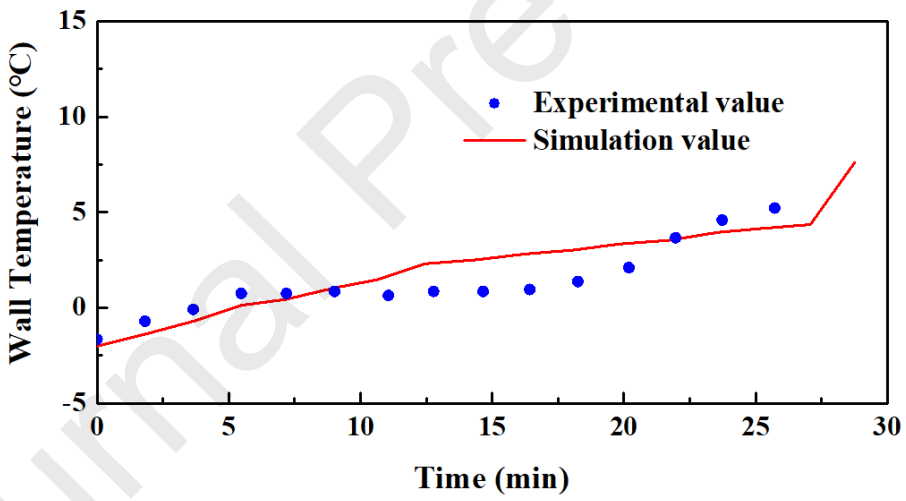

Figure 10: Comparison of monitored and predicted wall temperatures in the iron box

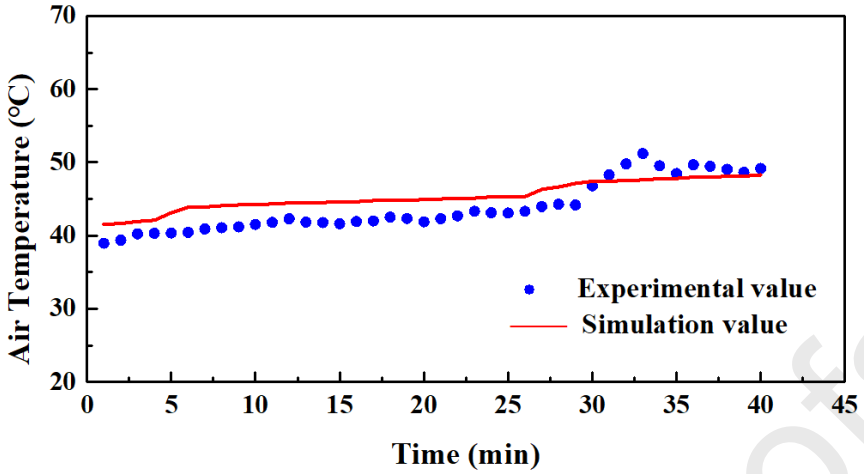

Figure 11: Comparison of monitored and predicted air temperatures in the enclosed hot-air melting system

2.2.5 Simulation conditions

Since the channel components allowed setting the maximum temperature, the maximum air supply temperature for the simulation was set at 75°C. Since the heater allowed setting the maximum air supply velocity, the maximum air supply velocity in the simulation was set as 13 m/s.

Due to its high porosity and low density, the density of new snow was between one-twelfth and one-fifth of solid ice, while the density of compacted snow was at least one-fifth of solid ice [30]. According to observations on the scene, there were many pores in the ice attached to the bottom of the train unit, with only a small amount of solid ice and much new snow or compacted snow. Therefore, it was more reasonable to use compacted snow when comparing ice melting time, and its density was one-fifth that of solid ice. In the remaining part of this paper, it is referred to as ice body.

The reference standard for the process of melting ice was liquid fraction, with an initial liquid fraction of 0 and a final liquid fraction of 1. The overall melting time was taken to be the time when the liquid fraction became 1.

3 Results

3.1 Convection melting

Table 2 shows the measured heat flux densities under different air supply conditions. When velocity was increasing, the heat flux caused by forced convection was increasing as well, complying with findings from existing studies [31-33].

Table 2. *Heat flux densities under different conditions (unit: W/m^2)*

	6 m/s	8 m/s	10 m/s	13 m/s
55°C	573	690	799	955
65°C	677	815	944	1129
75°C	782	941	1089	1303

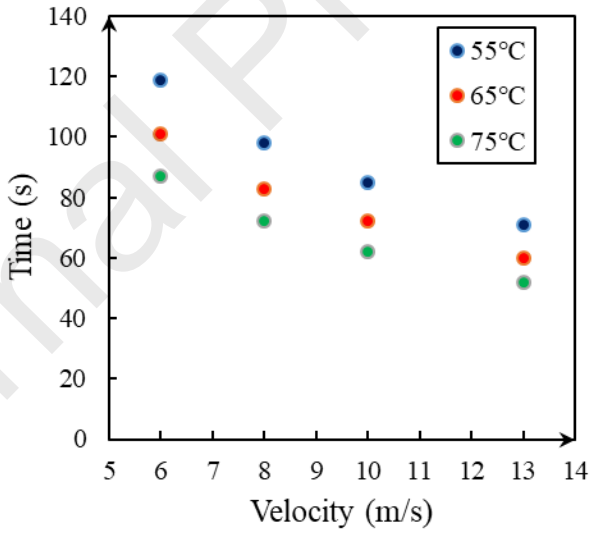

Figure 12: Comparison of melting time per millimeter of the ice body for different air supply conditions.

Figure 12 shows the ice melting time at different velocities. Different air supply

velocities of 6 m/s, 8 m/s, 10 m/s and 13 m/s were selected for the simulation to identify the influence of supply velocity on melting ice. The simulation results showed that the ice melting time was shorter at high velocity conditions, but there was no obvious linear correlation between melting time and velocity. When the velocity reached a certain level, the ice melting time did not change significantly with a further increase in velocity. In addition, increasing air supply flow excessively will result in significant waste of energy [34].

Different air supply temperatures, namely, 55°C, 65°C and 75°C, were selected to identify the influence of supply temperature on melting ice. Simulation results showed that when increasing the supply air temperature, the melting time was shortened accordingly, with a nearly linear relationship. Additionally, when increasing the supply air temperature, the energy consumed by the heaters increased significantly, which may impact the electrical components of the train chassis as well [35].

3.2 Gravity shedding melting

3.2.1 Iron box experiment and simulation

In the experiment, the ice body fell at 26 mins. To obtain the shedding time of the ice body in the simulation, it is necessary to investigate the critical condition of the falling time of the ice body. The critical condition for the ice body's falling means that the ice layer begins to fall after reaching a certain distance and a certain liquid fraction. The critical condition was estimated by the theoretical formula and corrected using both experimental results and simulation results. The theoretical formula is given by Equation 8.

$$a = \frac{qt}{\rho L} \tag{8}$$

where a is characteristic distance (m), the distance between the ice and the bottom of trains; q is heat flux density (W/m^2); t is time (s); ρ is density of ice body (kg/m^3); and L is latent heat of melting ice body (J/kg).

Using Equation 8, the characteristic distance was obtained as 0.29 mm. It was conservatively estimated that the characteristic distance of monitoring was 0.25 mm in the CFD simulation.

In the simulation, the average liquid fraction at the characteristic distance of 0.25 mm at 26 mins was 0.62; the average liquid fraction at the characteristic distance of 0.25 mm at 30 mins was 0.71; the average liquid fraction at the characteristic distance of 0.25 mm at 36 mins was 1. Due to the effect of gravity, the ice fell off before the liquid fraction became 1. The characteristic liquid fraction could be selected from the range 0.62 to 0.71. In this range, if the selected characteristic liquid fraction was larger, the probability that the ice body falls off the train body was larger. In this study, the characteristic liquid fraction was selected as 0.7.

The main purpose of the iron box experiment was to provide shedding critical conditions for the more complex model formulated in Section 3.2.2. In this study, the critical conditions for ice body shedding were defined as a characteristic distance of 0.25 mm and a liquid fraction of 0.7.

The liquid fractions in the central section of the iron box at different times in the simulation are shown in Figure 13.

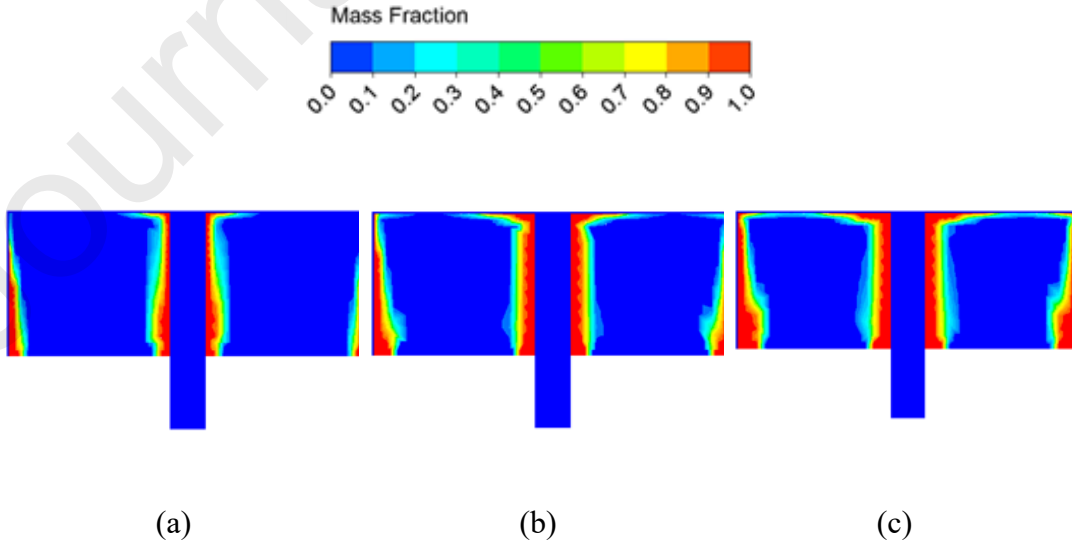

(a) (b) (c)

Figure 13. Liquid fraction at different times in the central section: (a) 10 min; (b) 20 min; (c) 30 min.

3.2.2 Simulation of the enclosed hot-air ice-melting system

For the gravity shedding study, the boundary set in the simulation was applied in experimental conditions, with temperature set at 65°C and air supply velocity set at 13 m/s. Figure 14 shows the monitored liquid fractions of the surface at different times.

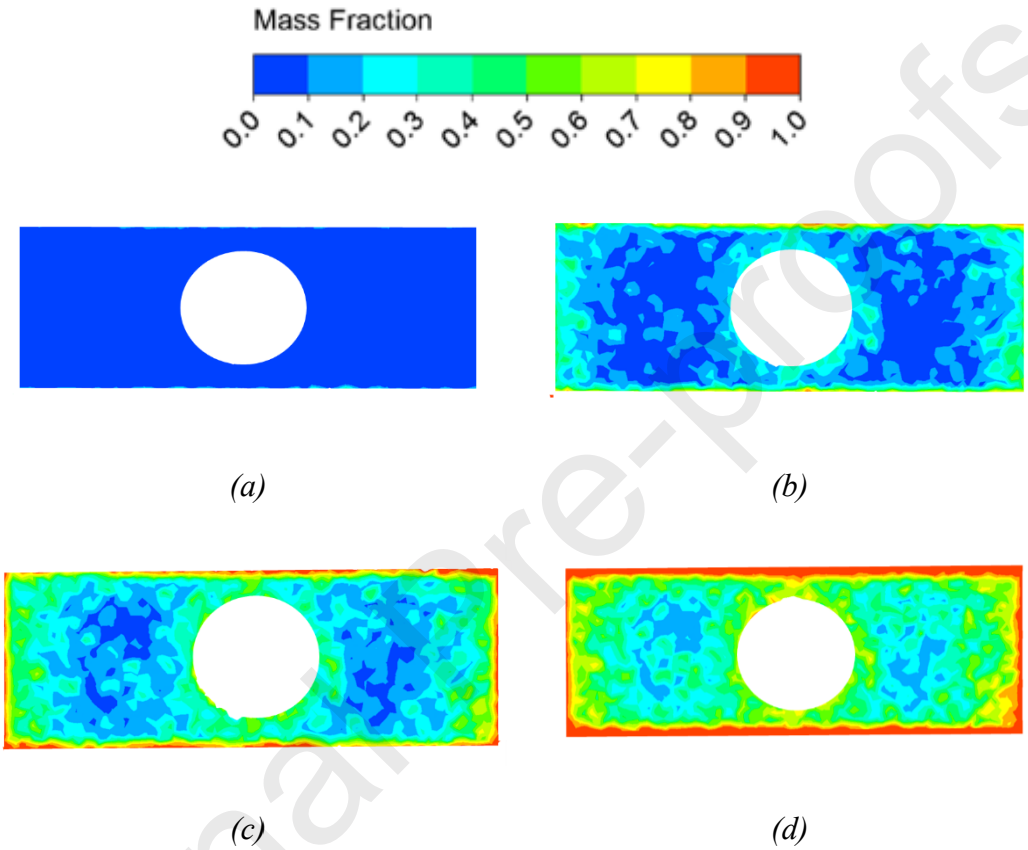

Figure 14: Liquid fraction of the monitored surface at different times. (a) 5 min; (b) 20 min; (c) 40 min; (d) 50 min.

In the simulation, the ice body shedding time was approximately 50 mins. Additionally, approximately 55 mins after the experiment began, it was observed that only a very small part of the ice body at the bottom of the train was not completely melted, and this part had to be knocked off manually.

4 Discussions

For the ice body, if it was melted only by natural convection melting, the speed of the melting process was found to be 1 mm/min, and only 50 mm could be melted within 50 mins. According to conservative estimates, an 80 mm ice body could fall off within 50 mins. Therefore, for thin ice bodies, convection melting is the dominant strategy, while for thick ice bodies, gravity shedding melting dominates.

4.1 Influential factors and improvement of the model for the convection melting of ice

4.1.1 Analysis of influential factors

For the train model with a vertical upward supply of air, an empirical formula for temperature and velocity versus heat flux density is given by Equation 9,

$$q = 14.34\log_{10} v(T_{in} - T_{ice}) \tag{9}$$

where q is heat flux density (W/m^2); v is vertical air supply velocity (m/s); T_{in} is temperature of the supply air (°C); and T_{ice} is initial temperature of the ice body (°C).

4.1.2 Model improvement

According to both experimental and simulation results, the horizontal velocity was only between 0.5 m/s and 1.3 m/s in the enclosed train body model, in which the heaters' air supply velocity was set at 13 m/s. In the improved model, the air supply direction was changed to horizontal, as shown in Figure 15.

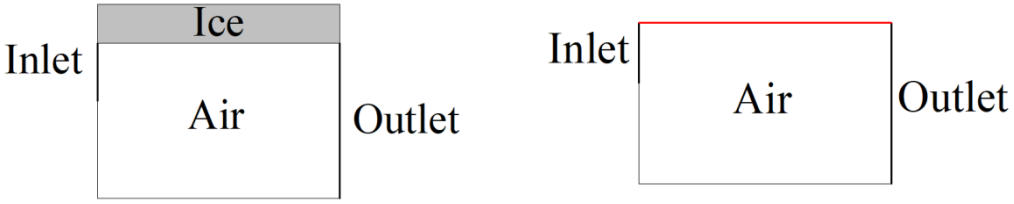

(a) *(b)*

Figure 15. Horizontal air supply model. (a) Schematic diagram of the model; (b) simulation calculation model. The red part is the interface between the ice and the air.

The heat flux densities under different working conditions are listed in Table 3.

Table 3. *Heat flux densities under different conditions of the horizontal air supply model (W/m²)*

	0.5 m/s	1 m/s	2 m/s	4 m/s	6 m/s	8 m/s
55°C	1094	1228	1245	1348	1464	1526
65°C	1289	1447	1466	1588	1725	1798
75°C	1483	1666	1688	1828	1986	2070

In the improved model (horizontal air supply), the air supply velocity was greatly reduced at the heat flux density closest to the actual model, resulting in reduced energy consumption.

For the improved model, an empirical formula for temperature and velocity versus heat flux density is given by Equation 10,

$$q = 30.66\log_{10} v(T_{in} - T_{ice}) \quad (10)$$

where q is heat flux density (W/m²); v is horizontal air supply velocity (m/s); T_{in} is temperature of the supply air (°C); and T_{ice} is initial temperature of the ice body (°C).

Therefore, the general empirical formula for heat flux density in ice melting conditions is given by Equation 11,

$$q = a\log_{10} v(T_{in} - T_{ice}) \quad (11)$$

where a is a constant related to the air supply model.

The heat flow density had a linear correlation with the temperature difference when the air supply velocity was kept constant. The heat flux density was logarithmically correlated with the air supply velocity when the supply air temperature difference was kept constant.

4.2 Energy analysis for the actual vertical air supply model

The energy performance of the system can be indicated by two important parameters, namely, heat energy and energy utilization factor, as defined in Equation 12 [36, 37] and Equation 13 [10], respectively.

$$Q = cm\Delta T \quad (12)$$

where Q is total system energy (kJ); c is specific heat capacity (kJ/kg·°C); m is mass of the supply air (kg); and ΔT is temperature difference (°C).

$$\eta = \frac{T_s - T_p}{T_s - T_n} \quad (13)$$

where η is energy utilization factor (-); T_s is supply air temperature (°C); T_p is exhaust air temperature (°C); and T_n is average air temperature in the working area (°C).

Table 4. *Comparison between the two systems*

	Supply air temperature (°C)	Exhaust air temperature (°C)	Average air temperature in the working area (°C)	Mass flow (kg/s)	Specific heat capacity (kJ/kg·°C)	Calculated energy (kW)	Actual energy (kW)	Energy utilization factor
Enclosed system	65.0	49.4	57.2	3.873	1.219	73.70	94.86	2.0
Unenclosed system [10]	60.0	52.8	54.4	5.880	1.219	51.61	—	1.3

Table 4 shows a comparison between the enclosed system and the unenclosed system in terms of both temperature and energy demand. In the CFD simulation results, according to Equation 12, the energy provided was 73.70 kW under experimental conditions (supply air at 65°C and 13 m/s). The average electricity consumption was 94.86 kW in the experiment. Due to the loss of electrical energy and heat loss caused by radiation, the energy consumption predicted by the simulation was less than the actual consumption. According to Equation 13, the energy utilization factor was calculated as 2.0 for the enclosed system. In comparison, the energy supplied to the train unit for melting ice was 51.61 kW, with an energy utilization factor of 1.3 under optimal conditions of the unenclosed system [10].

In summary, the enclosed hot-air ice-melting system can provide more energy and has a higher energy utilization coefficient than the unenclosed system. This can help to reduce energy consumption by nearly 50%.

4.3 The influence by physical parameters of the ice body

In reality, the geometry of ice body at the bottom of trains was irregular. This study has selected a thick ice body for investigation, and relevant geometrical information, such as thickness and shape may be different from the experimental setting here in real applications. Normally, the actual thickness of ice bodies in reality will be rarely higher than the tested thickness in this study. With a thinner ice body, the shedding time would be shorter, but with similar heat flux density if air supply conditions are not changing. In this study, a cuboid-shaped ice body has been selected but in reality the geometry may be in other forms, such as in inverted conical. This difference may lead to different contact areas, and hence different heat transfer efficiency. Additionally, ice bodies with different shapes may also have different gravity. These differences will then in turn affect the shedding time and the impact will be explored further in future studies.

5 Conclusions

The ice accumulated in a bogie chassis affects the stability of system operation, which

may cause serious safety issues. Therefore, solving this icing issue is extremely important for train transportation. Based on an enclosed hot-air melting system, this study investigated both natural convection ice melting and gravity shedding ice melting using experiment and simulation methods. This study has two main contributions: firstly, the study proposed a new method for calculating gravity shedding melting in complex models; secondly, the ice melting characteristics (heat flux, melting time) under different working conditions were provided for the design of the railway ice melting systems.

Obtained through both field experiments and CFD simulations, some main findings from this study are summarized as followings:

1) this study has confirmed the ice melting performance under different working conditions and has proposed a relationship between melting ice and heat flux density under natural convection melting;

2) through a combination of experiments and simulations, a new method for calculating gravity shedding melting in complex models has been adopted and validated;

3) a comparison between unenclosed and enclosed ice-melting systems revealed that the latter was much more energy efficient.

This study gives a good support of using enclosed systems for railway ice-melting, due to its advantages in both energy consumption and time. The heat flux of ice melting under different working conditions (based on simulation) identified in this paper can also be used to guide parameter selection of such systems to better fit requirements in field work. However, due to limitations in terms of available materials, labor and time, sufficient field measurements were not collected to validate the correlation established in this study (although the CFD simulation work has been calibrated), between supply air velocity and temperature difference between the inlets and the outlets of heaters. This work will be carried out in the future to strengthen the method introduced in this

paper.

Acknowledgment

The research in this paper was supported by the National Key R&D Program of the Ministry of Science and Technology, China, on "Green Buildings and Building Industrialization" through Grant No. 2018YFC0705300.

6 References

[1] N.R.A.o.t.P.s.R.o. China, 2017 Railway Statistics Bulletin, in, http://www.nra.gov.cn/xwzx/zlzx/hytj/201804/t20180412_55248.shtml, 2018.

[2] H. Shi, Research on De-icing and Anti-icing Technology for Trains and Wagons, Huazhong University of Science and Technology, 2013.

[3] B.S. AbdulNour, CFD prediction of automotive windshield defrost pattern, in, SAE Technical Paper, 1999.

[4] F. Xie, J. Zhang, G. Gao, K. He, Y. Zhang, J. Wang, Y. Zhang, Study of snow accumulation on a high-speed train's bogies based on the discrete phase model, J Appl Fluid Mech, 10 (6) (2017) 1729-1745.

[5] J. Wang, J. Zhang, F. Xie, Y. Zhang, G. Gao, A study of snow accumulating on the bogie and the effects of deflectors on the de-icing performance in the bogie region of a high-speed train, Cold Regions Science and Technology, 148 (2018) 121-130.

[6] L.R.R. Center, Benchmarking de-icing and anti-icing systems for trains and wagons and switches and crossings, in, Luleå University of Technology, 2011.

[7] M. Bettez, Winter technologies for high speed rail, Sweden: Norwegian University of Science and Technology, (2011).

[8] C. Ji, Experimental Research and Simulation Analysis for EMU De-icing Method, Tianjin University, 2012.

[9] X. Pu, The numerical simulation research of deicing system for Electric Multiple Unit, Tianjin University, 2017.

[10] C. Wu, J. Liu, H. Sun, Numerical Simulation of Airflow Organization of Ice-melting Air-Conditioning in Train Ice-melting Workshop, in: 2012 Railway HVAC Academic Annual Meeting, 2012.

[11] K. Katić, R. Li, J. Verhaart, W. Zeiler, Neural network based predictive control of personalized heating systems, Energy and Buildings, 174 (2018) 199-213.

[12] E. Foda, K. Sirén, Design strategy for maximizing the energy-efficiency of a localized floor-heating system using a thermal manikin with human thermoregulatory control, Energy and Buildings, 51 (2012) 111-121.

[13] S.B. Godithi, E. Sachdeva, V. Garg, R. Brown, C. Kohler, R. Rawal, A review of advances for thermal and visual comfort controls in personal environmental control (PEC) systems, Intelligent Buildings International, 11 (2) (2019) 75-104.

[14] Y. He, X. Wang, N. Li, M. He, D. He, Heating chair assisted by leg-warmer: A potential way to achieve better thermal comfort and greater energy conservation in winter, Energy and Buildings, 158 (2018) 1106-1116.

[15] B. Rezaie, M.A. Rosen, District heating and cooling: Review of technology and potential enhancements, Applied Energy, 93 (none) 2-10.

[16] I. Ansys, ANSYS FLUENT 13.0 Documentation, in, ANSYS Inc., Canonsburg, PA., 2009.

[17] C. Wang, J. Liu, W. Shang, H. Sun, J. Li, F. Fan, Experimental and numerical study of space station airflow distribution under microgravity condition, Building and Environment, 144 (2018) 268-280.

[18] Q. Chen, F. Rosner, A. Rao, S. Samuelsen, A. Jayaraman, G. Alptekin, Simulation of elevated temperature solid sorbent CO2 capture for pre-combustion applications using computational fluid dynamics, Applied energy, 237 (2019) 314-325.

[19] A. Kazemian, A. Salari, A. Hakkaki-Fard, T. Ma, Numerical investigation and parametric analysis of a photovoltaic thermal system integrated with phase change material, Applied Energy, 238 (2019) 734-746.

[20] M. Emam, M. Ahmed, Cooling concentrator photovoltaic systems using various configurations of phase-change material heat sinks, Energy conversion and management, 158 (2018) 298-314.

[21] T. A, FLUENT Tutorial guide, in: I. ANSYS (Ed.), 2015.

[22] A. Brent, V.R. Voller, K. Reid, Enthalpy-porosity technique for modeling convection-diffusion phase change: application to the melting of a pure metal, Numerical Heat Transfer, Part A Applications, 13 (3) (1988) 297-318.

[23] Y. Diao, L. Liang, Y. Zhao, Z. Wang, F. Bai, Numerical investigation of the thermal performance enhancement of latent heat thermal energy storage using longitudinal rectangular fins and flat micro-heat pipe arrays, Applied Energy, 233 (2019) 894-905.

[24] Z. Liu, Y. Yao, H. Wu, Numerical modeling for solid–liquid phase change phenomena in porous media: Shell-and-tube type latent heat thermal energy storage, Applied Energy, 112 (2013) 1222-1232.

[25] A. Farag, L.-J. Huang, CFD analysis and validation of automotive windshield de-icing simulation, in, SAE Technical Paper, 2003.

[26] Z.J. Zhai, Z. Zhang, W. Zhang, Q.Y. Chen, Evaluation of various turbulence models in predicting airflow and turbulence in enclosed environments by CFD: Part 1—Summary of prevalent turbulence models, Hvac&R Research, 13 (6) (2007) 853-870.

[27] Z. Zhang, W. Zhang, Z.J. Zhai, Q.Y. Chen, Evaluation of various turbulence models in predicting airflow and turbulence in enclosed environments by CFD: Part 2—Comparison with experimental data from literature, Hvac&R Research, 13 (6) (2007) 871-886.

[28] Q., Chen, Comparison of different k-ε models for indoor air flow computations, Numerical Heat Transfer Part B Fundamentals, (1995).

[29] X. Zhang, Performance analysis of automotive windshield defrosting, Shanghai Jiao Tong Universtiy 2007.

[30] P.P.H.w. group, Physical Practical Handbook, in: F.P.s.P. House (Ed.), 1991.

[31] S.M. Ammar, N. Abbas, S. Abbas, H.M. Ali, I. Hussain, M.M. Janjua, U. Sajjad, A. Dahiya, Condensing heat transfer coefficients of R134a in smooth and grooved multiport flat tubes of automotive heat exchanger: an experimental investigation, International Journal of Heat and Mass Transfer, 134 (2019) 366-376.

[32] Y. Chien-Yuh, N. Hamid, Condensation heat transfer and pressure drop of refrigerants HFO-1234yf and HFC-134a in small circular tube, International Journal of Heat & Mass Transfer, 127 (2018) 218-227.

[33] M. Li, G. Qiang, J. Lv, D. Li, Research on condensation heat transfer characteristics of R447A, R1234ze, R134a and R32 in multi-port micro-channel tubes, International Journal of Heat & Mass Transfer, 118 (mar.) (2018) 637-650.

[34] M. Bezovsky, M. Stricik, M. Prascakova, Energy demand and comparison of current defrosting technologies of frozen raw materials in defrosting tunnels, Applied Energy, 87 (8) (2010) 2447-2454.

[35] L. Fan, Numerical Simulation of the process of icing/melting, Nanjing University of Aeronautics and Astronautics, 2005.

[36] M. Amer, M.-R. Chen, U. Sajjad, H.M. Ali, N. Abbas, M.-C. Lu, C.-C. Wang, Experiments for suitability of plastic heat exchangers for dehumidification applications, Applied Thermal Engineering, 158 (2019) 113827.

[37] S.M. Ammar, N. Abbas, S. Abbas, H.M. Ali, I. Hussain, M.M. Janjua, Experimental investigation of condensation pressure drop of R134a in smooth and grooved multiport flat tubes of automotive heat exchanger, International Journal of Heat and Mass Transfer, 130 (2019) 1087-1095.

Author statement

Manuscript title: Experimental and numerical investigation of the performance of bogie chassis heater deicing systems

I have made substantial contributions to the conception or design of the work; or the acquisition, analysis, or interpretation of data for the work; AND

I have drafted the work or revised it critically for important intellectual content; AND I have approved the final version to be published; AND

I agree to be accountable for all aspects of the work in ensuring that questions related to the accuracy or integrity of any part of the work are appropriately investigated and resolved.

All persons who have made substantial contributions to the work reported in the manuscript, including those who provided editing and writing assistance but who are not authors, are named in the Acknowledgments section of the manuscript and have given their written permission to be named. If the manuscript does not include Acknowledgments, it is because the authors have not received substantial contributions from nonauthors.

Attachment: Yes No √

Author

Junjie Liu, Mingxin Liu, Diduo Liu, Baomin Huang, Zhaojun Sun, Shen Wei, Wenhua Chen, Xingli Pu

Date
5/19/2020